Targeted α-Therapy Using ^{225}Ac Radiolabeled Single-Domain Antibodies Induces Antigen-Specific Immune Responses and Instills Immunomodulation Both Systemically and at the Tumor Microenvironment

Thomas Ertveldt[1], Ahmet Krasniqi[2], Hannelore Ceuppens[1], Janik Puttemans[2], Yana Dekempeneer[2], Kevin De Jonghe[2], Wout de Mey[1], Quentin Lecocq[1], Yannick De Vlaeminck[1], Robin Maximilian Awad[1], Cleo Goyvaerts[1], Kim De Veirman[3], Alfred Morgenstern[4], Frank Bruchertseifer[4], Marleen Keyaerts[2,5], Nick Devoogdt[2], Matthias D'Huyvetter*[2], and Karine Breckpot*[1]

[1]*Department of Biomedical Sciences, Laboratory for Molecular and Cellular Therapy, Vrije Universiteit Brussel, Brussels, Belgium;* [2]*Department of Medical Imaging, In Vivo Cellular and Molecular Imaging Laboratory, Vrije Universiteit Brussel, Brussels, Belgium;* [3]*Department of Hematology and Immunology, Myeloma Center Brussels, Vrije Universiteit Brussel, Brussels, Belgium;* [4]*European Commission, Joint Research Centre, Directorate for Nuclear Safety and Security, Karlsruhe Institut, Germany; and* [5]*Department of Nuclear Medicine, UZ Brussel, Brussels, Belgium*

Targeted radionuclide therapy (TRT) using targeting moieties labeled with α-particle–emitting radionuclides (α-TRT) is an intensely investigated treatment approach as the short range of α-particles allows effective treatment of local lesions and micrometastases. However, profound assessment of the immunomodulatory effect of α-TRT is lacking in literature. **Methods:** Using flow cytometry of tumors, splenocyte restimulation, and multiplex analysis of blood serum, we studied immunologic responses ensuing from TRT with an antihuman CD20 single-domain antibody radiolabeled with ^{225}Ac in a human CD20 and ovalbumin expressing B16-melanoma model. **Results:** Tumor growth was delayed with α-TRT and increased blood levels of various cytokines such as interferon-γ, C-C motif chemokine ligand 5, granulocyte-macrophage colony-stimulating factor, and monocyte chemoattractant protein-1. Peripheral antitumoral T-cell responses were detected on α-TRT. At the tumor site, α-TRT modulated the cold tumor microenvironment (TME) to a more hospitable and hot habitat for antitumoral immune cells, characterized by a decrease in protumoral alternatively activated macrophages and an increase in antitumoral macrophages and dendritic cells. We also showed that α-TRT increased the percentage of programmed death-ligand 1 (PD-L1)–positive (PD-L1^{pos}) immune cells in the TME. To circumvent this immunosuppressive countermeasure we applied immune checkpoint blockade of the programmed cell death protein 1–PD-L1 axis. Combination of α-TRT with PD-L1 blockade potentiated the therapeutic effect, however, the combination aggravated adverse events. A long-term toxicity study revealed severe kidney damage ensuing from α-TRT. **Conclusion:** These data suggest that α-TRT alters the TME and induces systemic antitumoral immune responses, which explains why immune checkpoint blockade enhances the therapeutic effect of α-TRT. However, further optimization is warranted to avoid adverse events.

Key Words: actinium-225; immunology; oncology; single-domain antibody; radionuclide therapy

J Nucl Med 2023; 64:751–758
DOI: 10.2967/jnumed.122.264752

In patients with disseminated malignancies, targeted radionuclide therapy (TRT) holds promise for treatment of both primary lesions and micrometastases for which local radiotherapy is no longer applicable (*1*). In TRT, radiolabeled compounds are systemically administered to deliver radiation proximal to cancer cells. Therefore, tumor-targeting agents are coupled to α-, β^--, or Auger electron–emitting radionuclides (*2*). Various targeting modalities were developed and engineered to serve as TRT agents, with most prominent examples being radiolabeled monoclonal antibodies (mAbs), variants thereof and peptides (*3*). However, mAb-based TRT has been hampered by poor tissue penetration and myelosuppression as a result of bone marrow accumulation (*4,5*). So, the use of mAb fragments has been reassessed, leading to the development of single-domain antibodies (sdAbs), the antigen-binding fragments of heavy chain–only mAbs (*6*). SdAbs retain high affinity to their cognate epitope, with the additional benefit of binding to epitopes often inaccessible to mAbs. Hence, sdAbs have been extensively studied for many applications in the field of oncology, including imaging (*7*). Imaging studies have shown accumulation of sdAbs in local and disseminated cancer deposits with low background, a much-desired trait for TRT agents (*8*).

TRT with α-emitting radionuclides (α-TRT) is an intensely investigated treatment modality, as the short range of α-particles (<100 μm) allows effective treatment of local lesions and micrometastases with little to no crossfire (*1*). Because of the short range of α-particles, these were initially assumed to be of limited use in larger tumors and primarily intended for treatment of micrometastases. However, Kratochwil et al. described a reduction of tumor burden in patients with sizeable tumors (*9*). Whether this feature can be ascribed solely to the radiation aspect of α-TRT is up for debate as it has been shown that bystander immune activation contributes to the therapy outcome (*10*). Despite ongoing clinical

Received Aug. 10, 2022; revision accepted Dec. 6, 2022.
For correspondence or reprints, contact Karine Breckpot (Karine.Breckpot@vub.be).
*Contributed equally to this work.
Published online Apr. 13, 2023.

translation, immunologic changes as a result of α-TRT have not been studied in detail. To investigate immune involvement on α-TRT, we treated melanoma-bearing mice with sdAb-mediated α-TRT.

We used an immunocompetent mouse B16-melanoma model expressing the transgenes human complex of differentiation 20 (huCD20) and ovalbumin to assess the outcome and immune-modifying properties of α-TRT performed with well-characterized antihuCD20 sdAb 9079 labeled with ^{225}Ac (*11*). We analyzed tumor cell targeting in vivo and the ability of the therapy to delay tumor growth. Systemic effects on ^{225}Ac-9079 were studied through analysis of serum cytokine levels and tumor specificity of $CD8^{pos}$ splenocytes. The tumor microenvironment (TME) was analyzed by flow cytometry to assess tumor-infiltrating immune cells and their expression of inhibitory immune checkpoint ligands and receptors. Furthermore, we ventured into immuno-α-TRT, where we supplemented the ^{225}Ac-9079 treatment regimen with immune checkpoint blockade (ICB) of the programmed cell death protein 1 (PD-1)–programmed death-ligand 1 (PD-L1) axis. Finally, we assessed the radiation burden in the long term in healthy mice 4 mo after administration of ^{225}Ac-9079.

MATERIALS AND METHODS

Cell Line

Mycoplasma-free huCD20 transgenic B16-melanoma cells (B16-huCD20) were provided by Jan Tavernier (VIB-UGent). These were cultured and tested for antigen expression and cell surface expression of huCD20 as previously described (*11*).

sdAb and ^{225}Ac Radiolabeling

SdAb 9079 binds huCD20 and serves as a targeting moiety for TRT in the B16-huCD20 model (*11*). SdAb R3B23 binds the M protein of 5T2MM cells and was used as a nontargeting control sdAb throughout this study (*12*). Carrier-free ^{225}Ac (DG Joint Research Centre) was conjugated to sdAbs using 2-(4-isothiocyanatobenzyl)-1,4,7,10-tetraazacyclododecane-1,4,7,10-tetraacetic acid (DOTA; Macrocyclics). Radiochemical purity was evaluated using instant thin-layer chromatography. [^{225}Ac]Ac-DOTA-sdAbs with a radiochemical purity of more than 95% and molar activity of 78.8 and 158.9 kBq/nmol were used for therapy and biodistribution purposes, respectively. Henceforth, [^{225}Ac]Ac-DOTA-9079 will be referred to as ^{225}Ac-9079, [^{225}Ac]Ac-DOTA-R3B23 as ^{225}Ac-R3B23, and [^{225}Ac]Ac-DOTA-sdAbs as ^{225}Ac-sdAbs.

Animal Model

C57BL/6 mice (Charles River) were transplanted subcutaneously in the right thigh with $10E^5$ B16-huCD20 cells. Experiments were performed in accordance with the European guidelines for animal experimentation and approved by the ethical committee for use of laboratory animals of the Vrije Universiteit Brussel.

Ex Vivo Biodistribution of ^{225}Ac-sdAbs and Dosimetry

Mice bearing subcutaneous tumors of 250 ± 100 mm^3 were injected intravenously with a single injection of 25 kBq (±5.0 μg) of ^{225}Ac-9079 or ^{225}Ac-R3B23 coinfused with Gelofusine (150 mg/kg) (*13*). Various organs, tissues, and tumors were isolated and weighed, and their level of radioactivity was analyzed using a γ-counter (Wizard^2; Perkin Elmer). Results were expressed as percentage injected activity per gram of tissue. Next, the absorbed doses were calculated by multiplying the obtained residence time with the corresponding S value.

Therapy

For the therapy experiments studying α-TRT as a stand-alone therapy, mice received 3 repeated intravenous injections of 52.8 ± 1.7 kBq or 98.1 ± 4.7 kBq of ^{225}Ac-9079 (±3.3 μg) on days 3, 9, and 14 of subcutaneous B16-huCD20 tumor growth, with a cumulative radioactive dose of 180 kBq or 300 kBq, respectively. Control mice received 3 repeated intravenous injections of 95.8 ± 4.6 kBq of ^{225}Ac-R3B23 (±3.3 μg), with a cumulative radioactive dose of 300 kBq. All mice had palpable subcutaneous tumors when therapy started.

A similar set-up was used for immuno-TRT therapy in which α-TRT was combined with ICB. Mice received repeated intravenous injections of 98.1 ± 4.7 kBq of ^{225}Ac-9079 (±3.3 μg) on days 3, 6, and 15 of subcutaneous B16-huCD20 tumor growth, with a cumulative radioactive dose of 300 kBq. ICB was performed by intraperitoneal administration of 100 μg/injection of antibody on days 7, 10, 14, and 17. Antimurine PD-L1 blocking antibody (RRID:AB_2800597), rat IgG2b, κ isotype control (IC) antibody (RRID:AB_11149687), antimurine PD-1 blocking antibody (RRID:AB_2800576), and rat IgG2a, κ IC antibody (RRID:AB_11149687) were used.

Acute Serum Cytokine Analysis

To analyze the immediate inflammatory response to α-TRT on serum cytokine levels, blood was collected 6 h after the last treatment. Cytokine content was determined using the Bio-Plex Pro Mouse Cytokine 23-plex Assay (RRID:AB_2857368).

Single Cell Suspensions

Tumors were mechanically dissected and enzymatically digested by an enzyme mix of DNase I (Sigma-Aldrich), Dispase II (Roche), and Collagenase I (Sigma-Aldrich) to obtain a single cell suspension. Red blood cell lysis was performed using NH_4Cl-Tris solution.

Flow Cytometry

Surface antigen staining was performed on single-cell suspensions preincubated with anti-CD16/32 antibodies (RRID:AB_312801) and a live/dead marker (LIVE/DEAD Fixable Green Dead Cell Stain Kit; Thermo Fisher Scientific). Cells were washed and stained with 2 antibody panels binding CD45.2 (RRID:AB_1727492), CD3ε (RRID:AB_2737945), CD4 (RRID:AB_396956), CD8α (RRID:AB_394081), CD11b (RRID:AB_396960), CD11c (RRID:AB_2725779), CD206 (RRID:AB_10895754), PD-L1 (RRID:AB_2738911), PD-L2 (RRID:AB_2739947), PD-1 (RRID:AB_394284), F4/80 (RRID:AB_2743450), Ly6G (RRID:AB_1727560), and MHC-II (RRID:AB_2565979). Cells were acquired on the Celesta flow cytometer (BD Biosciences) and analyzed using the FlowJo X software (RRID:SCR_008520; BD Biosciences). t-SNE plots arising from this process were generated using the FlowJo X software.

Restimulation of Splenocytes

Spleens were mashed through a 40-μm cell strainer (Falcon) and transferred to a tube containing RPMI1640 medium, after which cells were stimulated for 48 h with 100 pmol of peptides (Anaspec). As a control, splenocytes were cultured in RPMI1640 medium. ELISA (enzyme-linked immunosorbent assay) was performed on culture supernatant to measure interferon (IFN)-γ in supernatant (mouse IFN-γ ELISA; Invitrogen).

Statistical Analysis

Kaplan–Meier curves showing the time to reach humane endpoints were statistically analyzed using log-rank (Mantel–Cox) and Gehan–Breslow–Wilcoxon tests. One-way ANOVA was performed for all other results and corrected for multiple comparisons via Tukey's multiple-comparisons correction. All statistical analyses were conducted in GraphPad Prism 9.3.1 (GraphPad Software). Sample sizes (n) and the number of times experiments were repeated (N) are indicated in the figure legends. The asterisks in the figures indicate the

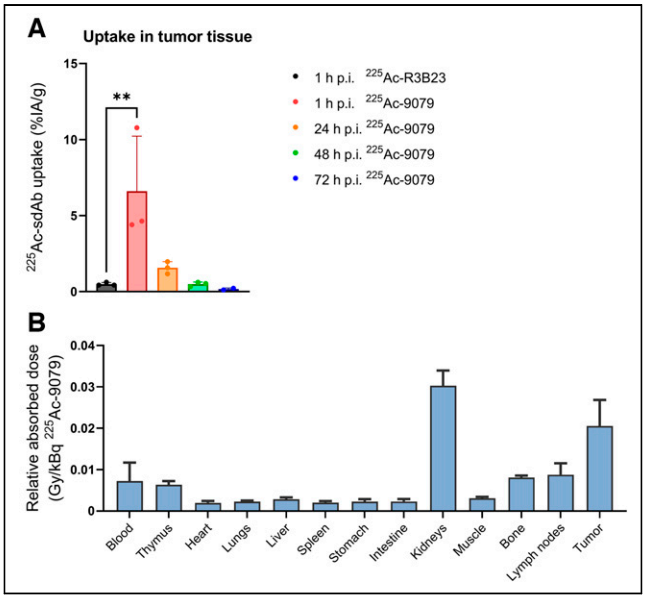

FIGURE 1. Ex vivo biodistribution data show accumulation of ^{225}Ac-9079 in B16-huCD20 tumors. (A) Tumor uptake of ^{225}Ac-9079 and ^{225}Ac-R3B23 was quantified at 1, 24, 48, and 72 h after injection and 1 h after injection, respectively ($N = 1$, $n = 2$–3 per time point). Bar graph shows individual values with grouped mean ± SD. (B) Tissue dosimetry on administration of ^{225}Ac-9079 was performed using trapezoid exponential fitting with grouped mean ± SD ($N = 1$, $n = 3$). %IA/g = percentage injected activity per gram of tissue; p.i. = after injection.

level of statistical significance (*$P < 0.05$; **$P < 0.01$; ***$P < 0.001$; ****$P < 0.0001$). Nonsignificant changes are not indicated.

Data Availability Statement

The data generated in this study are available within the article and the supplemental files (supplemental materials are available at http://jnm.snmjournals.org). Biodistribution files, multiplex data, and flow cytometry files are available on request from the corresponding author.

RESULTS

^{225}Ac-9079 Specifically Accumulates in B16-huCD20 Tumors

We evaluated accumulation of ^{225}Ac-9079 in B16-huCD20 tumor and tissues that do not express huCD20 at 1, 24, 48, and 72 h after intravenous injection. Mice injected with ^{225}Ac-R3B23 were euthanized at 1 h after injection for comparison. B16-huCD20 tumors showed a significant accumulation of ^{225}Ac-9079, yet not ^{225}Ac-R3B23, at 1 h after injection ($P < 0.0061$) (Fig. 1A). We observed little uptake and retention over time of ^{225}Ac-9079 in nontumor tissues, with the exception of the kidneys via which sdAbs are excreted from the body. Dosimetry calculations showed an absorbed dose delivered to B16-huCD20 tumors than that to the spleen, bone marrow and other tissues (excluding kidneys) (Fig. 1B).

^{225}Ac-9079 Delays B16-huCD20 Tumor Growth

Mice injected subcutaneously in the thigh with B16-huCD20 cells were randomized 3 d after injection to receive a cumulative dose of 180 or 300 kBq of ^{225}Ac-9079. Fractionated treatment was given on days 3, 9, and 14 after tumor cell inoculation, resulting in delivery of a cumulative absorbed dose of 4 or 6 Gy to B16-huCD20 tumors, respectively (Supplemental Fig. 1A). For comparison, mice received a cumulative dose of 300 kBq of ^{225}Ac-R3B23. Tumor growth was delayed when mice were treated with 300 kBq of ^{225}Ac-9079 ($P = 0.0148$; Fig. 2A). This therapeutic effect translated into an increased time to reach humane endpoints in mice treated with 180 or 300 kBq of ^{225}Ac-9079 ($P = 0.0236$ and $P = 0.0014$, respectively; Fig. 2B). No evidence of acute, systemic treatment-related toxicity was observed, as indicated by the animals' body weight (Fig. 2C).

Peripheral Immune Responses Suggest Antigen-Specific Immune Activation on Treatment with ^{225}Ac-9079

We analyzed 23 cytokines in serum collected at 6 h after the last treatment to address the immune activating potential of α-TRT. All cytokines, except for interleukin (IL)-3, were detected in blood samples (Fig. 3A; Supplemental Fig. 2). Statistical tests compared ^{225}Ac-9079 conditions with ^{225}Ac-R3B23, with P values displayed separately in Supplemental Table 1. Cytokine serum levels of IL-1β, IL-10, tumor necrosis factor (TNF)-α, keratinocyte chemoattractant (KC), IFN-γ, C-C motif chemokine Ligand 5 (CCL5), monocyte chemoattractant protein-1 (MCP-1), and granulocyte-macrophage colony-stimulating factor (GM-CSF) were significantly upregulated in both ^{225}Ac-9079 conditions (Fig. 3A; Supplemental Fig. 2). The serum levels of IL-4, IL-12(p40), and granulocyte colony-stimulating factor (G-CSF) were significantly increased only in mice administered 300 kBq of ^{225}Ac-9079 (Fig. 3A; Supplemental Fig. 2). The serum levels of IL-9 and macrophage inflammatory protein (MIP)-1α were significantly increased only in mice administered 180 kBq of ^{225}Ac-9079 condition (Fig. 3A; Supplemental Fig. 2). No significant changes were observed for the cytokines IL-1α, IL-2, IL-5, IL-6, IL-12p70, IL-13, IL-17, eotaxin, MIP-1β (Fig. 3A; Supplemental Fig. 2).

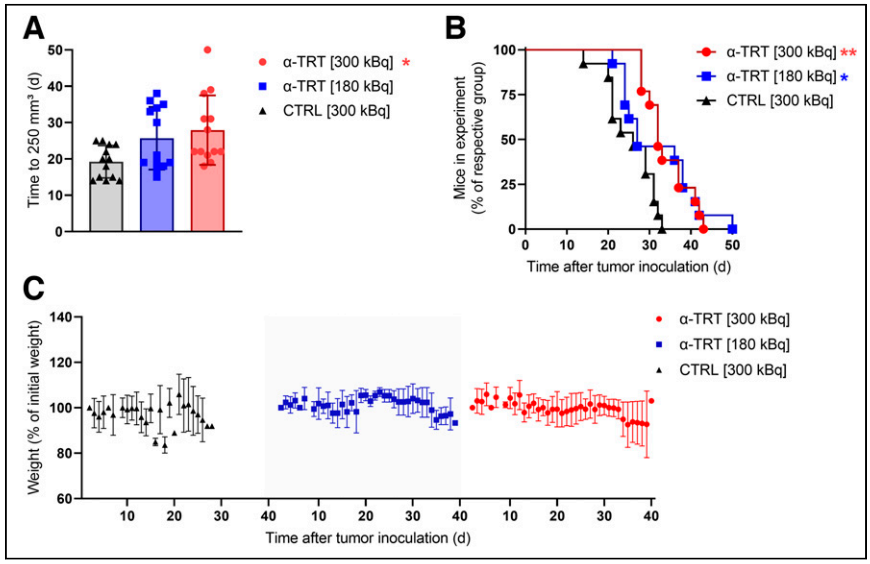

FIGURE 2. Therapy with ^{225}Ac-9079 impedes tumor growth. (A) Pooled times to reach tumor volume of 250 mm^3 are shown by group. Bar graph shows individual values with grouped mean ± SD. (B) Pooled Kaplan–Meier curve showing time at which mice reached humane endpoints. (C) Pooled weight of treated mice over course of time. Graph shows grouped mean ± SD ($N = 2$, $n = 6$). CTRL = ^{225}Ac-labeled nontargeting sdAb.

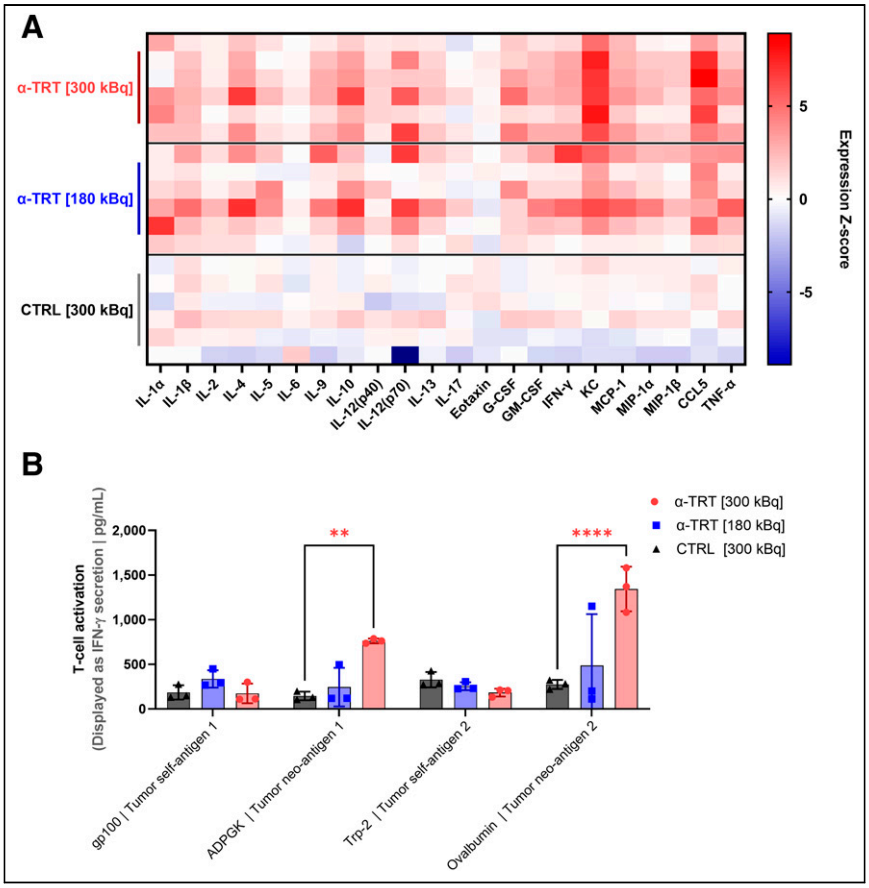

FIGURE 3. Peripheral immune responses suggest immune activation on treatment with ^{225}Ac-9079. (A) Multiplex analysis of cytokine levels 6 h after last administration of ^{225}Ac-sdAbs. Heatmap is generated using z-transformed cytokine levels ($N = 1$, $n = 6$). (B) Analysis of IFN-γ production by splenocytes stimulated with cancer antigen–derived peptides. Graph shows individual values with grouped mean ± SD ($N = 1$, $n = 3$). CTRL = ^{225}Ac-labeled nontargeting sdAb; G-CSF = granulocyte colony-stimulating factor; GM-CSF = granulocyte-macrophage colony-stimulating factor; KC = keratinocyte chemoattractant; TNF-α = tumor necrosis factor-α.

CD8^{pos} splenocytes were stimulated with peptides, derived from antigens expressed by B16-huCD20 tumor cells, including the 2 melanoma differentiation antigens glycoprotein 100 $(gp100)_{25–33}$ and tyrosinase-related protein 2 $(Trp2)_{181–188}$ next to 2 model neoantigens: ADP dependent glucokinase $(ADPGK)_{299–307}$ and ovalbumin$_{257–264}$. Production of IFN-γ, a measure of T-cell activation, was demonstrated only in mice treated with 300 kBq of ^{225}Ac-9079 in response to ADPGK and ovalbumin ($P = 0.0019$ and $P < 0.0001$, respectively) (Fig. 3B). In contrast, we were unable to show IFN-γ induction on stimulation with gp100 or Trp2 peptides.

^{225}Ac-9079 Modulated the TME to Favor Antitumoral Cells

B16-huCD20 tumors were isolated when they reached 250 ± 100 mm^3. Single-cell suspensions of these tumors were subjected to flow cytometry analysis to study the tumor immune signature (Supplemental Figs. 3 and 4). Statistical tests compared ^{225}Ac-9079 conditions with ^{225}Ac-R3B23, and P values are displayed separately in Supplemental Table 2. Multicolor flow cytometry analyses of TME showed a similar T-cell count and no major differences among T-cell subpopulations (Fig. 4A). PD-1-expression on CD4^{pos} T-cells was significantly upregulated in tumors of mice treated with ^{225}Ac-9079 (Fig. 4B; Supplemental Fig. 5B).

Among tumor-infiltrating myeloid cells, the significant decrease in total myeloid numbers coincided with a significant decrease in protumoral alternatively activated macrophages (M2) in tumors treated with ^{225}Ac-9079 (Fig. 5A; Supplemental Fig. 5E). Furthermore, a significant increase in antitumoral classically activated macrophages (M1) and dendritic cells (DCs) was also observed in tumors treated with ^{225}Ac-9079 (Fig. 5A; Supplemental Figs. 5F and 5G). Within the immune cells, we observed that PD-L1 was significantly increased on cDC2s and M1 macrophages residing in tumors treated with ^{225}Ac-9079 (Fig. 5B; Supplemental Fig. 5H). No difference in expression level was observed for inhibitory immune checkpoint ligand PD-L2 (Fig. 5B).

PD-L1 Checkpoint Blockade Further Reduces Tumor Growth After ^{225}Ac-9079 Therapy Yet Coincides with Severe Weight Loss

Mice injected subcutaneously in the thigh with B16-huCD20 cells were randomized 3 d after injection to receive a cumulative dose of 300 kBq of ^{225}Ac-9079 on days 3, 6, and 15 intravenously or 100 μg of mAbs on days 7, 10, 14, and 17 intraperitoneally after tumor cell inoculation (Supplemental Fig. 1B). Tumor growth was delayed when mice were treated with 300 kBq of ^{225}Ac-9079 combined with PD-L1 but not with PD-1 ICB (Fig. 6A). However, administration of both ^{225}Ac-9079 and PD-L1 ICB resulted in extensive weight loss, which was not observed with the combination of ^{225}Ac-9079 and PD-1 ICB (Fig. 6B).

Long-Term Toxicity Study Reveals Organ Damage After α-TRT with ^{225}Ac-9079

Healthy mice received a single injection of 300 kBq of ^{225}Ac-9079 or phosphate-buffered saline and were monitored until month 4 after treatment, at which time mice treated with ^{225}Ac-9079 showed a weight loss of 20% or more (Supplemental Fig. 1C). All mice were euthanized, and organs of interest were isolated and weighed. Liver, heart, and lungs displayed a minor reduction in weight, whereas the mass of the spleen and kidneys was significantly reduced by 29.5% ± 4.3% ($P = 0.0011$) and 65.5% ± 1.8% ($P < 0.0001$) in mice treated with ^{225}Ac-9079 (Fig. 7).

DISCUSSION

In this study, we showed that α-TRT with ^{225}Ac-9079 in the B16-huCD20 melanoma mouse model has therapeutic potential as it delays tumor growth. We further showed stimulation of cytokine release, tumor-specific CD8^{pos} T-cell responses, and a shift from a tumor-promoting TME to a TME characterized by an immune contexture that enables tumor cell rejection, including activated (PD-1^{pos}) T-cells, classically activated macrophages, and DCs. Finally, we showed that ICB with anti-PD-L1 mAbs combined with α-TRT improves tumor control compared with either therapy alone, albeit coinciding with adverse events (i.e., weight loss).

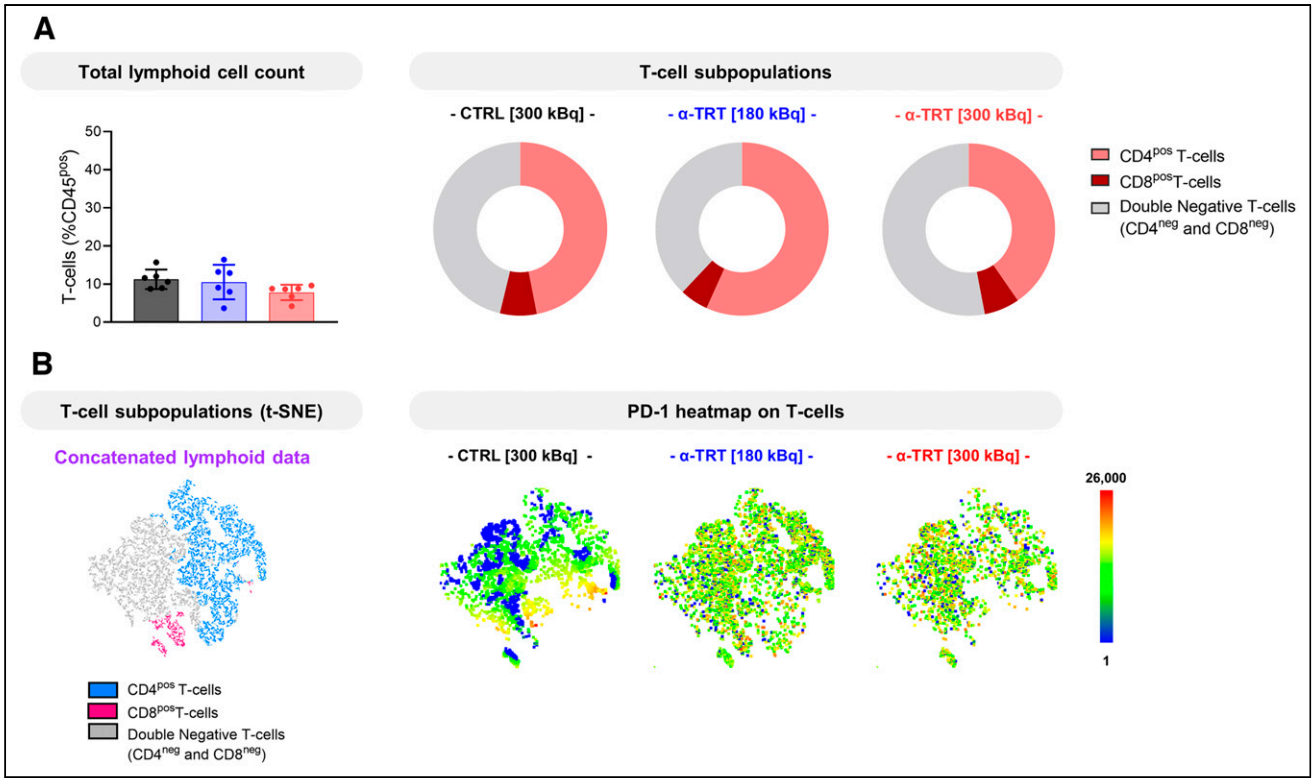

FIGURE 4. α-TRT increased PD-1 expression on tumoral CD4^{pos} T-cells. (A) Composition of T-cell subpopulations, among T-cells. (B) Concatenated t-distributed stochastic neighbor embedding (t-SNE) plot of the T-cell lineage, overlayed with T-cell subpopulations. Concatenated t-SNE heatmaps show expression of PD-1 on T-cell subpopulations per treatment group. Heatmap range represents marker mean fluorescence intensity (MFI). Graph shows individual values with grouped mean ± SD ($N = 1$, $n = 6$). CTRL = ^{225}Ac-labeled nontargeting sdAb.

We evaluated the potential of ^{225}Ac-9079 as an α-TRT agent and showed specific accumulation in B16-huCD20 tumors of immunocompetent mice, sparing muCD20^{pos} cells. This observation is in line with previous work performed with the same sdAb, albeit conjugated to another linker and radionuclide (*11*). For therapeutic efficacy, a dose approximating 5 Gy was desired as literature described little therapeutic effect given solid tumors' resilience to radiation (*14*). Hence 180 and 300 kBq of ^{225}Ac-9079 were administered, corresponding to respective delivery of 4 and 6 Gy in tumor. The observed delay in tumor growth with ^{225}Ac-9079 is in line with published studies that highlight the potential of ^{225}Ac as a therapeutic radionuclide (*9*).

Serum cytokine levels were quantified as markers for systemic immune activation, and various cytokines were enhanced. Increased levels of MCP-1 and GM-CSF suggest monocytes or macrophage migration or infiltration and DC maturation, respectively (*15,16*). Furthermore, elevation of antitumoral cytokines such as IFN-γ and CCL5 advocates activation of CD8^{pos} T-cells and serves as predictor of response to ICB (*17*). A recent study investigating adoptive cell transfer and α-TRT described the secretion CCL5 and IFN-γ from tumor on treatment (*18*). These results prompted us to restimulate isolated spleens with cancer-associated epitopes. Intriguingly, IFN-γ secretion revealed that splenocytes recognized and reacted to ADPGK and ovalbumin but not toward melanoma differentiation antigens. Evidence of high-avidity antitumoral CD8^{pos} T-cells responses on α-TRT has not yet been published.

After analyzing systemic responses, we evaluated α-TRT–mediated alteration of the TME, which is emphasized by an increase in professional antigen presenting cells at the expense of immunosuppressive subsets of myeloid cells. More specifically, alternatively activated macrophages (M2) are significantly decreased in numbers. These cells are involved in wound healing under physiologic conditions and attenuating immune responses to prevent collateral tissue damage (*19*). In malignancy, M2 macrophages are enthralled by tumor cells to overexert immunosuppressive functions, quench uprising antitumoral responses, and facilitate tumor progression and metastasis (*19*). Unlike, M2 macrophages, we documented an increase in M1 macrophages and DCs, professional antigen presenting cells involved in the education of T-cell responses (*20*). This observation is consistent with the cytokine profile of MCP-1 and GM-CSF, hinting at macrophage infiltration and DC maturation. DCs can acquire antigens, migrate, and present these to T-cells within lymph structures to elicit a clonal T-cell response, which ties in with the identification of antitumoral T-cells in the spleen (*21*). Regarding the expression pattern of immune checkpoint receptors in the TME, we noted that α-TRT upregulated expression of PD-1 on CD4^{pos} T-cells as well as its ligand, PD-L1, on various cell types in the TME. In recent studies involving α-TRT, a similar observation was made (*18*). Ligation of PD-1 to PD-L1 impairs T-cell receptor signaling, in turn interfering with the effector function of antitumoral T-cells (*20*). In short, we observed that ^{225}Ac-9079 altered the tumor immune compartment, favoring myeloid cells that likely facilitate antigen processing, presentation, and education of T-cell responses, were it not for the presence of inhibitory markers such as PD-1 and PD-L1. To overcome this hurdle we performed ICB of the PD-1–PD-L1 axis to enhance the therapeutic effect of sdAb-mediated α-TRT.

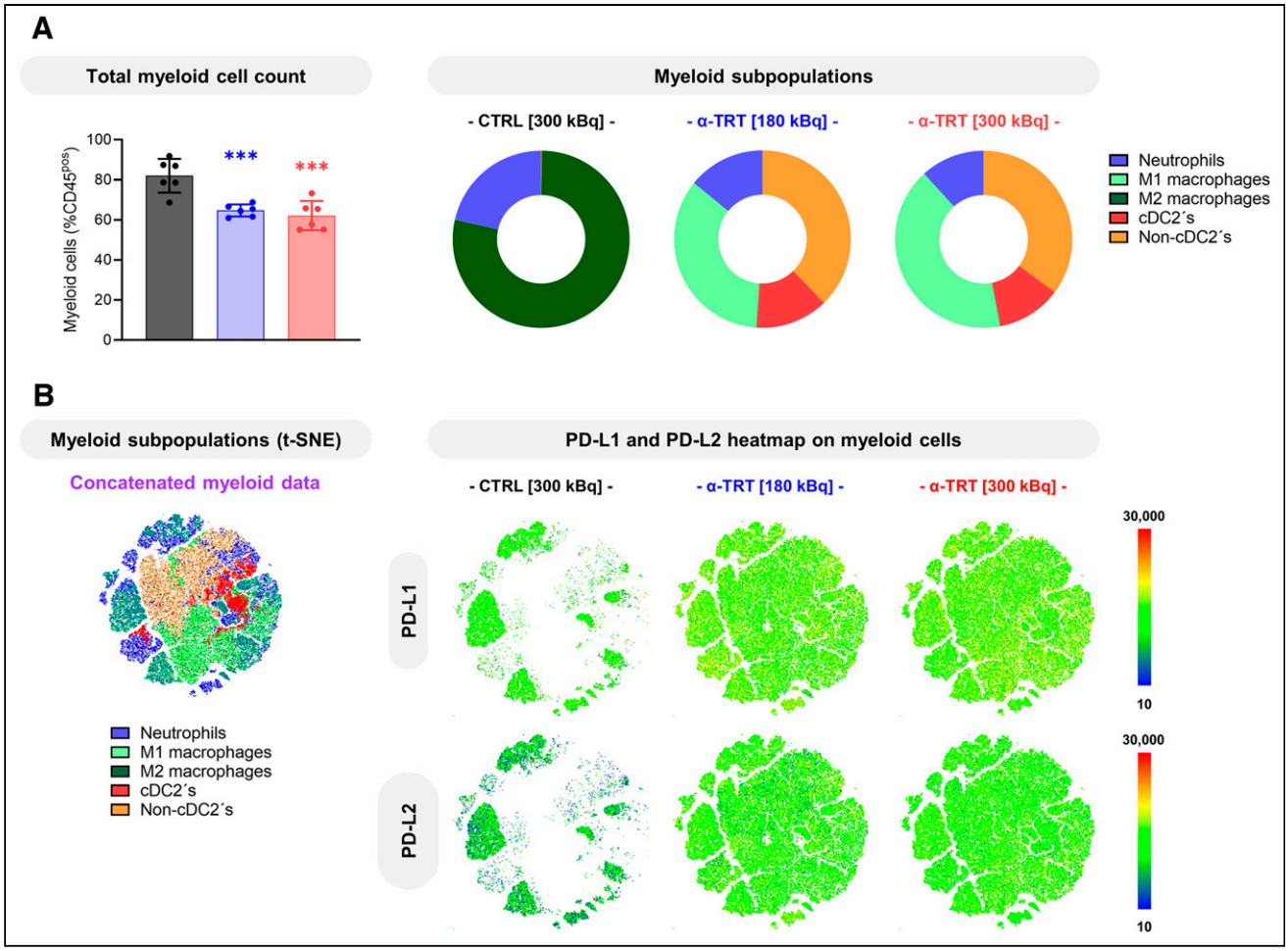

FIGURE 5. α-TRT reduced M2 macrophage and increased M1 macrophage and DC count in tumor tissue. (A) Composition of myeloid subpopulations among myeloid cells. (B) Concatenated t-SNE plot of myeloid lineage, overlayed with myeloid subpopulations. Concatenated t-SNE heatmaps showing expression of PD-L1 and PD-L2 on myeloid subpopulations per treatment group. Heatmap ranges represent marker mean fluorescence intensity (MFI). Graph shows individual values with grouped mean ± SD ($N = 1, n = 6$). CTRL = ^{225}Ac-labeled nontargeting sdAb.

Synergy between α-TRT and ICB occurred only in combination with PD-L1 blockade in these experiments, despite literature stating PD-1 synergizes with α-TRT as well (*22*). Intriguingly, PD-L1 ICB on its own did not amount to a therapeutic effect, compared with the IC, whereas PD-1 had therapeutic benefit on its own. We surmise that PD-L1 ICB after α-TRT is this effective because of the immune alterations induced on α-TRT, setting the stage to unleash all this immunologic potential. Besides the effect of anti-PD-L1 mAbs as a blocking agent, antibody-dependent cellular cytotoxicity (ADCC) also comes into play. Unlike the PD-1 mAb, the PD-L1 mAb used in this study is able to induce ADCC (*23*). Hence, we surmised that PD-L1^{pos} tumor and stromal cells in the TME are clad with mAbs on PD-L1 ICB, flagging them for ADCC by FcγR^{pos} effector cells, such as B cells, NK cells, and M1 macrophages, which highly infiltrate tumors subjected to α-TRT (*24*). Unfortunately, mice that received a combination of α-TRT and PD-L1 ICB experienced extensive weight loss, resulting in premature attainment of a humane endpoint. We presume that this phenomenon is the result of the combination therapy's ensuing cytokine storm as mice receiving a similar amount of radioactivity or ICB, as monotherapy, did not lose weight during the course of the experiment. Curiously, α-TRT with PD-1 ICB did not result in weight loss, suggesting the onset of ADCC by the PD-L1 mAb may have played a crucial role in this process.

To investigate late-stage systemic radiation burden, we administered similar therapeutic doses to healthy mice, which allowed long-term follow up. We noted that 4 mo after administration of ^{225}Ac-9079, mice started losing weight. The spleen and kidneys of these mice were severely reduced in size compared with unirradiated mice, suggesting that α-TRT inflicted severe damage to these organs. Damage to tubular epithelial cells and loss of renal function on α-TRT was described by Scheinberg et al. (*25*). Unlike the kidneys, spleen biodistribution data does not advocate for a substantial accumulation of ^{225}Ac-9079. Hence, we surmise that the loss of spleen weight is not directly related to the radiation aspect and is more likely a systemic effect due to the extensive weight loss. Cheal et al. demonstrated that injection of 296 kBq of ^{225}Ac is tolerated by mice; however, the study relied on a pretargeted approach using haptens, resulting in minimal kidney retention (*26*). With about 10 times the size of a hapten, a 15 kDa sdAb is excreted via the kidneys' glomerulus with moderate retention, resulting in kidneys being the dose-limiting organ of sdAb-mediated TRT.

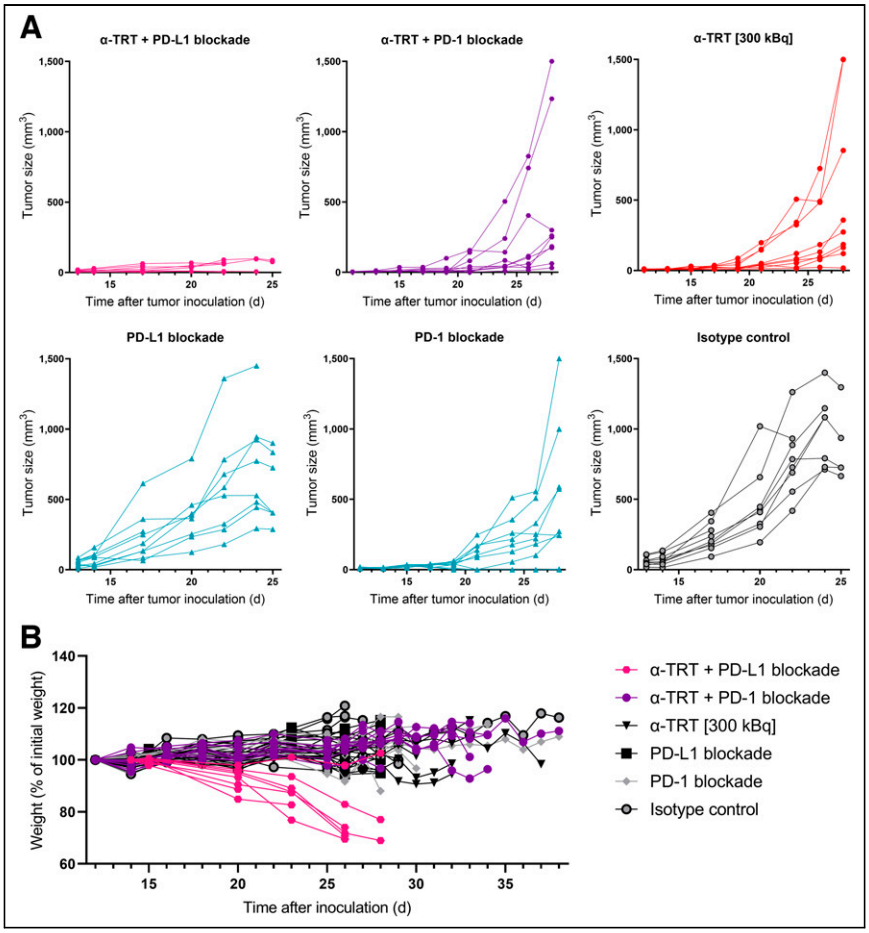

FIGURE 6. Therapy with ^{225}Ac-9079 acts in synergy with immune checkpoint blockade but potentiates adverse effects. (A) Grouped tumor kinetics are shown during course of experiment by individual mouse. (B) Weight of treated mice during course of experiment, displayed as individual values ($N = 1$, $n = 9$).

Hence, the pretargeting approach is worthwhile investigating to circumvent the limitations imposed by the kidneys for sdAb-mediated TRT (*27*). Other possible avenues are modulation of sdAb protein sequence, cleavable linkers, and novel coupling methods to avoid a high radiation burden on the kidneys (*28*). In this regard, a limitation of this study is the lack of histologic evaluation of kidneys, which would have yielded more insight into the extent of renal damage inflicted upon α-TRT. Furthermore, immune analyses were performed at a single time point. Though this provided valuable insights, it might not reflect the dynamic nature of the immune system and its contribution to immune-related adverse events. Finally, the antihuCD20 sdAb used in this study does not bind mouse CD20, thus introducing a bias in the healthy organ dosimetry. However, antihuCD20 TRT using mAbs was previously performed in patients and displayed an acceptable safety profile (*5*).

Future perspectives for ameliorating the therapeutic index of α-TRT consists of combination strategies to reduce the radiation burden on dose-limiting organs such as kidneys as well as titration of ICB. Further tweaking of the therapy regimen should circumvent kidney damage as well as immune-related adverse events.

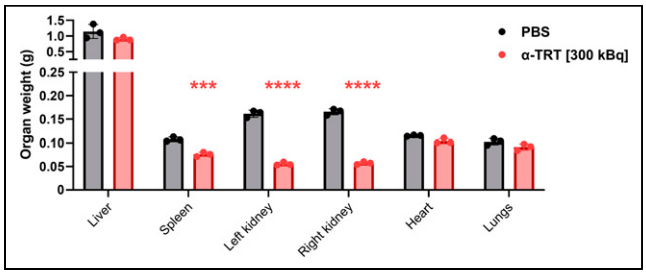

FIGURE 7. Long-term toxicity study reveals major organ damage 4 mo after administration of ^{225}Ac-sdAbs. Weight of whole isolated organs, 4 mo after administration of ^{225}Ac-9079 or phosphate-buffered saline (PBS). Bar graph shows individual datapoints and grouped mean ± SD ($N = 1$, $n = 3$).

CONCLUSION

To our knowledge, this is the first study addressing immune activation in a melanoma model on α-TRT with ^{225}Ac-sdAbs. Our findings suggest that α-TRT alters the TME and induces systemic antitumoral immune responses, which in turn were unhinged via ICB to enhance therapeutic effect but warrants further optimization because of synergistic adverse effects.

DISCLOSURE

This research was supported by the Belgian Foundation against Cancer (2016–076/FAF-F/2016/798); Kom op tegen Kanker (Stand-up to Cancer); the Flemish Cancer Society and the Research Council of the Vrije Universiteit Brussel (Strategic Research Program 48 and 62). Furthermore, Thomas Ertveldt and Robin Maximilian Awad are PhD fellows funded via the Research Foundation-Flanders (FWO-V, grants 1S06622N and 1S05020N, respectively). Yannick De Vlaeminck, Quentin Lecocq, and Janik Puttemans were supported by FWO-V during the execution of this work (1S24817N, 1S24220N and I001618N, respectively). Marleen Keyaerts and both Matthias D'Huyvetter and Kim De Veirman are, respectively, senior clinical investigator (1801619N) and postdoctoral fellows (12H3619N and 12I0921N) of FWO-V. The BD Celesta flow cytometer was funded via an FWO-Hercules grant (I001618N). Karine Breckpot, Nick Devoogdt, Matthias D'Huyvetter, Marleen Keyaerts, Ahmet Krasniqi, and Quentin Lecocq have patents on the use of single-domain antibodies. Nick Devoogdt and Marleen Keyaerts have ownership in AbScint, which leverages sdAb imaging tracers into clinical application. Marleen Keyaerts received research funding from Precirix, a biotech company that develops novel radiopharmaceuticals. Nick Devoogdt and Matthias D'Huyvetter are, respectively, consultant and employee for and hold ownership in Precirix. No other potential conflict of interest relevant to this article was reported.

KEY POINTS

QUESTION: Does α-TRT result in a sufficient release of immunologic cues to induce systemic antigen-specific T-cell responses?

PERTINENT FINDINGS: Upon restimulation of spleens with cancer-associated peptides, we observed a significant T-cell activation, suggesting that α-TRT can induce tumor-specific immunity toward immunogenic neoantigens.

IMPLICATIONS FOR PATIENT CARE: Induction of T-cell responses with α-TRT implies that synergistic immunologic applications enhance the therapeutic effect by potentiating antitumoral T-cells. Hence, combination trials gain in interest, especially at the advent of pembrolizumab (PD-1 blocking mAb) being approved for treatment of non-Hodgkin lymphoma and various other malignancies.

REFERENCES

1. Pouget JP, Constanzo J. Revisiting the radiobiology of targeted alpha therapy. *Front Med (Lausanne).* 2021;8:692436.
2. Turner JH. An introduction to the clinical practice of theranostics in oncology. *Br J Radiol.* 2018;91:20180440.
3. Gill MR, Falzone N, Du Y, Vallis KA. Targeted radionuclide therapy in combined-modality regimens. *Lancet Oncol.* 2017;18:e414–e423.
4. Scott AM, Wolchok JD, Old LJ. Antibody therapy of cancer. *Nat Rev Cancer.* 2012;12:278–287.
5. Witzig TE, White CA, Gordon LI, et al. Safety of yttrium-90 ibritumomab tiuxetan radioimmunotherapy for relapsed low-grade, follicular, or transformed non-Hodgkin's lymphoma. *J Clin Oncol.* 2003;21:1263–1270.
6. Muyldermans S. Nanobodies: natural single-domain antibodies. *Annu Rev Biochem.* 2013;82:775–797.
7. Awad RM, Meeus F, Ceuppens H, et al. Emerging applications of nanobodies in cancer therapy. *Int Rev Cell Mol Biol.* 2022;369:143–199.
8. Keyaerts M, Xavier C, Heemskerk J, et al. Phase I study of ^{68}Ga-HER2-nanobody for PET/CT assessment of HER2 expression in breast carcinoma. *J Nucl Med.* 2016;57:27–33.
9. Kratochwil C, Bruchertseifer F, Giesel FL, et al. ^{225}Ac-PSMA-617 for PSMA-targeted α-radiation therapy of metastatic castration-resistant prostate cancer. *J Nucl Med.* 2016;57:1941–1944.
10. Brady D, O'Sullivan JM, Prise KM. What is the role of the bystander response in radionuclide therapies? *Front Oncol.* 2013;3:215.
11. Ertveldt T, de Beck L, de Ridder K, et al. Targeted radionuclide therapy with low and high-dose Lutetium-177 labeled single domain antibodies induces distinct immune signatures in a mouse melanoma model. *Mol Cancer Ther.* 2022;21:1136–1148.
12. Lemaire M, D'Huyvetter M, Lahoutte T, et al. Imaging and radioimmunotherapy of multiple myeloma with anti-idiotypic Nanobodies. *Leukemia.* 2014;28:444–447.
13. D'Huyvetter M, Vincke C, Xavier C, et al. Targeted radionuclide therapy with a 177 Lu-labeled anti-HER2 nanobody. *Theranostics.* 2014;4:708–720.
14. Patel RB, Hernandez R, Carlson P, et al. Low-dose targeted radionuclide therapy renders immunologically cold tumors responsive to immune checkpoint blockade. *Sci Transl Med.* 2021;13:eabb3631.
15. Inaba K, Inaba M, Romani N, et al. Generation of large numbers of dendritic cells from mouse bone marrow cultures supplemented with granulocyte/macrophage colony-stimulating factor. *J Exp Med.* 1992;176:1693–1702.
16. Deshmane SL, Kremlev S, Amini S, Sawaya BE. Monocyte chemoattractant protein-1 (MCP-1): an overview. *J Interferon Cytokine Res.* 2009;29:313–326.
17. Karachaliou N, Gonzalez-Cao M, Crespo G, et al. Interferon gamma, an important marker of response to immune checkpoint blockade in non-small cell lung cancer and melanoma patients. *Ther Adv Med Oncol.* 2018;10.
18. Perrin J, Capitao M, Allard M, et al. Targeted alpha particle therapy remodels the tumor microenvironment and improves efficacy of immunotherapy. *Int J Radiat Oncol Biol Phys.* 2022;112:790–801.
19. Awad RM, de Vlaeminck Y, Maebe J, Goyvaerts C, Breckpot K. Turn back the TIMe: targeting tumor infiltrating myeloid cells to revert cancer progression. *Front Immunol.* 2018;9:1977.
20. Peng Q, Qiu X, Zhang Z, et al. PD-L1 on dendritic cells attenuates T cell activation and regulates response to immune checkpoint blockade. *Nat Commun.* 2020;11:4835.
21. Chiang MC, Tullett KM, Lee YS, et al. Differential uptake and cross-presentation of soluble and necrotic cell antigen by human DC subsets. *Eur J Immunol.* 2016;46:329–339.
22. Czernin J, Current K, Mona CE, et al. Immune-Checkpoint Blockade Enhances ^{225}Ac-PSMA617 efficacy in a mouse model of prostate cancer. *J Nucl Med.* 2021;62:228–231.
23. Dahan R, Sega E, Engelhardt J, Selby M, Korman AJ. Ravetch J v. FcγRs modulate the anti-tumor activity of antibodies targeting the PD-1/PD-L1 axis. *Cancer Cell.* 2015;28:285–295.
24. Nimmerjahn F. Ravetch J v. Translating basic mechanisms of IgG effector activity into next generation cancer therapies. *Cancer Immun.* 2012;12:13.
25. Scheinberg DA, McDevitt MR. Actinium-225 in targeted alpha-particle therapeutic applications. *Curr Radiopharm.* 2011;4:306–320.
26. Cheal SM, McDevitt MR, Santich BH, et al. Alpha radioimmunotherapy using ^{225}Ac-proteus-DOTA for solid tumors: safety at curative doses. *Theranostics.* 2020;10:11359–11375.
27. Cheal SM, Chung SK, Vaughn BA. Cheung NK v., Larson SM. Pretargeting: a path forward for radioimmunotherapy. *J Nucl Med.* 2022;63:1302–1315.
28. Chigoho DM, Bridoux J, Hernot S. Reducing the renal retention of low- to moderate-molecular-weight radiopharmaceuticals. *Curr Opin Chem Biol.* 2021;63:219–228.